Catalysis Today xxx (xxxx) xxx–xxx

Contents lists available at ScienceDirect

Catalysis Today

journal homepage: www.elsevier.com/locate/cattod

CO adsorption, reduction and oxidation on $Pb(Zr,Ti)O_3(001)$ surfaces associated with negatively charged gold nanoparticles

Nicoleta G. Apostol[a], Marius A. Huanu[a], Daniel Lizzit[b], Ioana A. Hristea[a,c], Cristina F. Chirilă[a], Lucian Trupină[a], Cristian M. Teodorescu[a,*]

[a] National Institute of Materials Physics, Atomiștilor 405A, 077125 Măgurele, Ilfov, Romania
[b] Elettra Sincrotrone Trieste, S.S. 14 – km 163, 5, Area Science Park, 34169 Basovizza, Trieste, Italy
[c] University of Bucharest, Faculty of Physics, Atomiștilor 405, 077125 Măgurele, Ilfov, Romania

ARTICLE INFO

Keywords:
Ferroelectric surfaces
Carbon monoxide
Gold nanoparticles
Adsorption
Desorption
Photoelectron spectroscopy

ABSTRACT

Gold is deposited on atomically clean, inwards polarized, ferroelectric lead zirco-titanate deposited by pulsed laser deposition on strontium titanate (001) single crystal, then carbon monoxide adsorption and desorption experiments are investigated by *in situ* fast photoelectron spectroscopy using synchrotron radiation. Atomic force microscopy and high resolution photoelectron spectroscopy are consistent with the formation of 50–100 nm nanoparticles, and their Au 4f core levels point to a negative charge state of gold. As compared with a similar experiment performed on ferroelectric lead zirco-titanate with similar polarization state and without gold, the saturation coverage after exposure to carbon monoxide increases by about 68 %, and also most of the additional carbon is found in oxidized state. Desorption experiments with *in situ* follow-up by photoelectron spectroscopy are performed as function of temperature, and the neutral carbon intensity decreases when the ferroelectric polarization decreases, while the components corresponding to oxidized carbon remain unchanged. It looks that neutral carbon adsorption is strictly related to the polarization of the ferroelectric film, while carbon still found in molecular form is related to its carbonyl bonding on metal nanoparticles, independent of the polarization state of the substrate. Desorbed carbon at higher temperature uptakes oxygen from the substrate.

1. Introduction

Surface reactions involving carbon monoxide are of actual interest since almost a century, owing to the harmfulness of this molecule, the necessity to remove it from the exhaust gases, or to convert it into fuels *via* Fischer–Tropsch synthesis or methanation [1]. An important point regards the fixation of this molecule on the surface of a catalyst, together with the ability to dissociate it and to ensure a sufficient surface mobility of the resulting fragments, manifested in the well-known 'volcano plot' of optimal conditions for catalysis [1,2]. Ferroelectric materials, whose polarization may be easily switched by external parameters (electric fields, strain or temperature), provide the ability to modulate adsorption or desorption energies [2,3], including the proposition to cycle their polarization such as to explore both sides of the 'volcano' (large binding energy to attach reactants alternating with low binding energy to release products) [4]. Chemical and catalytic activity of ferroelectric surfaces are actively investigated since almost two decades [5,6]; however, only recently experiments on CO adsorption on a ferroelectric surface have been performed in ultraclean conditions on well-defined surfaces from stoichiometric and structural points of view, with well characterized polarization orientations and follow-up in real time of adsorption/desorption processes [7]. The main results from this previous work were: (i) a straightforward correlation between the amount of CO adsorbed and the polarization state of the substrate, (ii) evidence for considerable dissociation of the molecule upon its fixation on the ferroelectric surface; (iii) carbon release from the surface in the form of CO_2 with temperature increase up to the loss of the surface ferroelectric polarization. This is in line with previous results concerning noticeable differences in adsorption energetics of CO or CO_2 on ferroelectric surfaces [6,8–10].

In fact, for adsorption of polar or polarizable molecules on ferroelectric surfaces with out-of-plane polarization, several aspects have to be taken into account. The basic argument is of electrostatic nature and invokes the energetics of the dipole interaction with the electric field promoted by the material. From this point of view, CO has a very weak dipole moment, oriented from C to O, hence C is slightly more negative at the equilibrium. However, unidirectional anisotropic polarizability of this molecule implies the easier induction by an external field of a

* Corresponding author.
E-mail address: teodorescu@infim.ro (C.M. Teodorescu).

https://doi.org/10.1016/j.cattod.2020.02.042
Received 28 August 2019; Received in revised form 16 January 2020; Accepted 28 February 2020

dipole oriented from oxygen towards carbon than in the opposite direction [7]. As a consequence, carbon becomes the positive ion in the molecular dipole and will be attached on a surface with an inwards oriented electric field (negative fixed charges), and this explains the previous findings from Ref. [7]. When we speak about larger polar molecules, especially about alcohols or acids with an anionic head and a cationic tail (i. e. negative charge localized and positive charge delocalized on the tail or in a more extended spatial region), these anionic heads are likely to be attached on areas with outwards polarization (positive fixed charges), and this was also demonstrated in several previous works [11,12].

However, electrostatic arguments may be used when there is a sizeable electric field outside the material [13] to be perceived by molecules in gas phase or in solutions. Several charge compensation mechanisms could interfere and yield to the lowering, up to the vanishing of the external electric field. Extrinsic charge compensation in liquids builds up a Stern layer [14] or polarized solid-liquid interfaces without voltage applied [15], whereas, in gas phase or at solid surfaces in vacuum, contaminants may play a similar role [9,16]. In absence of extrinsic compensation, compensation by charge generated inside the ferroelectric build up charge sheets in the immediate neighborhood of the external surfaces [16–18]. Moreover, a detailed account of atomic structure reveals atomic reconstructions, manifested by deviations from stoichiometry in the first atomic layer [5,8,19], and this is accompanied by electronic reconstructions [8]. Microstructural effects and their interplay with polarization must also be taken into account [20]. Sometimes a net result was obtained such as the independence of chemisorption energy on the polarization, or adsorption mechanisms stemming in physisorption [21]; note that more recent work pointed on a clear dependence of adsorption energies or on activation energies for desorption on temperature or on the polarization state of the substrate [2,7,11,19]. To complicate further the problem, indirect [4,7] or direct [22] evidence for oxygen uptake from the material for desorption in form of CO_2 was reported. CO_2 uptake even on a top metal electrode was found to influence the value of the polarization of a thin ferroelectric film [23]. Finally, as a process essentially important for photocatalysis, but more generally applicable, in the case of intrinsic screening, charge carrier (holes or electrons) transfer towards the surface *via* the near surface band bending in the material yields to an increase in carrier lifetime with respect to recombination [24] and generates active species (·OH and O_2–, respectively) for surface redox processes [12,13,25–27]. Ionic migration due to polarization effects near interfaces was also inferred and found to interfere with molecular adsorption [28,29].

Putting everything together, the expected efficiency of ferroelectric catalysts is promising, albeit often beyond expectation regarding reproducibility and reaction rates [9]. ‘Traditional’ catalysts for CO–related reactions are noble metals (Pd, Pt), owing, amongst others, to the complex charge transfer (donation from σ electrons to the metal, back-donation of d electrons from the metal into antibonding π* orbitals) occurring when CO is adsorbed on them [30]. A natural choice is to combine noble metals with ferroelectric surfaces and, indeed, the first results were quite promising, e. g. in achieving a rate of almost 100 % CO oxidation at temperatures of 350 K [3]. Other effects presumably due to synergies between noble metal and ferroelectrics include enhanced photocatalysis [13], photochemical growth of noble metal nanoparticles [6,25] or electric fields at metal-ferroelectric Schottky-like interfaces helping charge separation [9,31]. Still in debate are the influence of surface plasmons on influencing photocatalysis using visible light [13,32]. Also, noble metal (Au) nanoparticles were detected in negatively charged states upon their deposition on ferroelectric surfaces [31,33] and one expects that these charge states will drastically influence the back-donation and the dissociation pathways of adsorbed molecules.

To mitigate all effects difficult to be quantified, such as pre-contamination, surface inhomogeneities, complicated polarization landscape or surface decomposition [34–36], experiments on well-defined surfaces, single domain, reasonably clean before CO dosing must be carried out, following the example of Ref. 7. X-ray photoelectron spectroscopy (XPS), through its ability to discriminate between different ionic or bonding state of surface atoms or molecules [26,37] combined with the ability to derive surface band bending and assess locally the polarization states [7,15,33–35,38] is the ideal tool for these investigations. In this work we present a follow-up by *in situ*, time and temperature dependent XPS of CO adsorption and desorption of a Pb(Zr,Ti)O_3(001) (PZT) surface with gold nanoparticles pre-deposited on it. These nanoparticles are visualized by *ex situ* atomic force microscopy. With respect to Ref. 7, a higher amount of carbon monoxide is found to adsorb, but with a lower dissociation rate. Gold is found in a negative ionization state, similar to the findings of Refs. 27 and 33, and this state is proposed to enhance the catalytic activity of the heterosurface.

2. Experimental

PZT films (atomic content ratio Zr:Ti = 1:4) of 50 nm thickness are synthesized on 20 nm $SrRuO_3$(001) (SRO) conductive buffer layers grown on $SrTiO_3$(001) by pulsed laser deposition (PLD). All films are routinely characterized by atomic force microscopy (AFM) and X-ray diffraction (XRD). XRD patterns for films similar to the ones used in this work may be found in Fig. 1(a), magenta curve, from Ref. [[39]. A clear (001) orientation of these films is derived from these patterns. Also, Fig. 3 (a) from Ref. [[39] presented clear rectangular ferroelectric polarization–voltage loops. Synthesis details are now standard in the community of PLD growers of perovskite thin films and largely described in Ref. 33, for example. The thickness of 50 nm was chosen as being close to the upper limit for single domain out-of-plane polarization [[[39]. The dosing and *in situ* characterization experiments were performed in the CoSMoS facility connected to the SuperESCA beamline at the Elettra synchrotron radiation facility in Trieste. Photon energies of 260 eV for Pb 4f, Au 4f and Zr 3d, 400 eV for C 1s and of 680 eV for Ti 2p and O 1s were used, such as to avoid overlapping with Auger lines and to have similar escape depth for photoelectrons originating from different core levels. XPS using also a monochromatized Al K_α X-ray gun was performed, to check the derived compositions, since in this case the incident beam intensity is constant and the atomic sensitivity factors are well known. Photoelectrons are detected at a takeoff angle of 24 degrees, by using a 150 mm radius Phoibos hemispherical electron energy analyzer operating in “medium area” mode with pass energy of 10 eV for synchrotron radiation experiments and 30 eV for conventional XPS. Energy calibration is achieved by cross-checks between the Fermi level of a Ni(111) single crystal, the Au 4f level and the Fermi level for a thick (about 3 nm) gold film deposited on a degenerated semiconducting sample. This was performed at all photon energies used in this experiment.

PZT films were loaded in ultrahigh vacuum (UHV, base pressure 10^{-8} Pa) and checked by XPS as introduced, then after a cleaning procedure consisting in annealing during four hours at 400 °C in 0.005 Pa of molecular oxygen [7]. Gold was deposited from a carefully outgassed Createc cell (situated in a separate chamber for molecular beam epitaxy, base pressure into 10^{-9} Pa) at a rate of 1 Å min^{-1}, in a pressure of 5.0×10^{-7} Pa. The samples were characterized also after gold deposition, then carbon monoxide was dosed at room temperature in the main (analysis) chamber at a pressure of 0.005 Pa for 20 min, hence dosing about 4.5×10^4 L (45 kL), where 1 L = 10^{-6} Torr × 1 s. Then, all core levels were measured while heating the sample, up to the loss of out-of-plane polarization, as followed by the position of core levels. Desorption induced by synchrotron radiation was recorded, similar to the findings from Ref. 7. Repeated dosing and desorption follow-up experiments allowed one to infer that the above dose is fairly close to saturation. For the computation of the carbon coverage corresponding to this saturation (at room temperature), see the next Section.

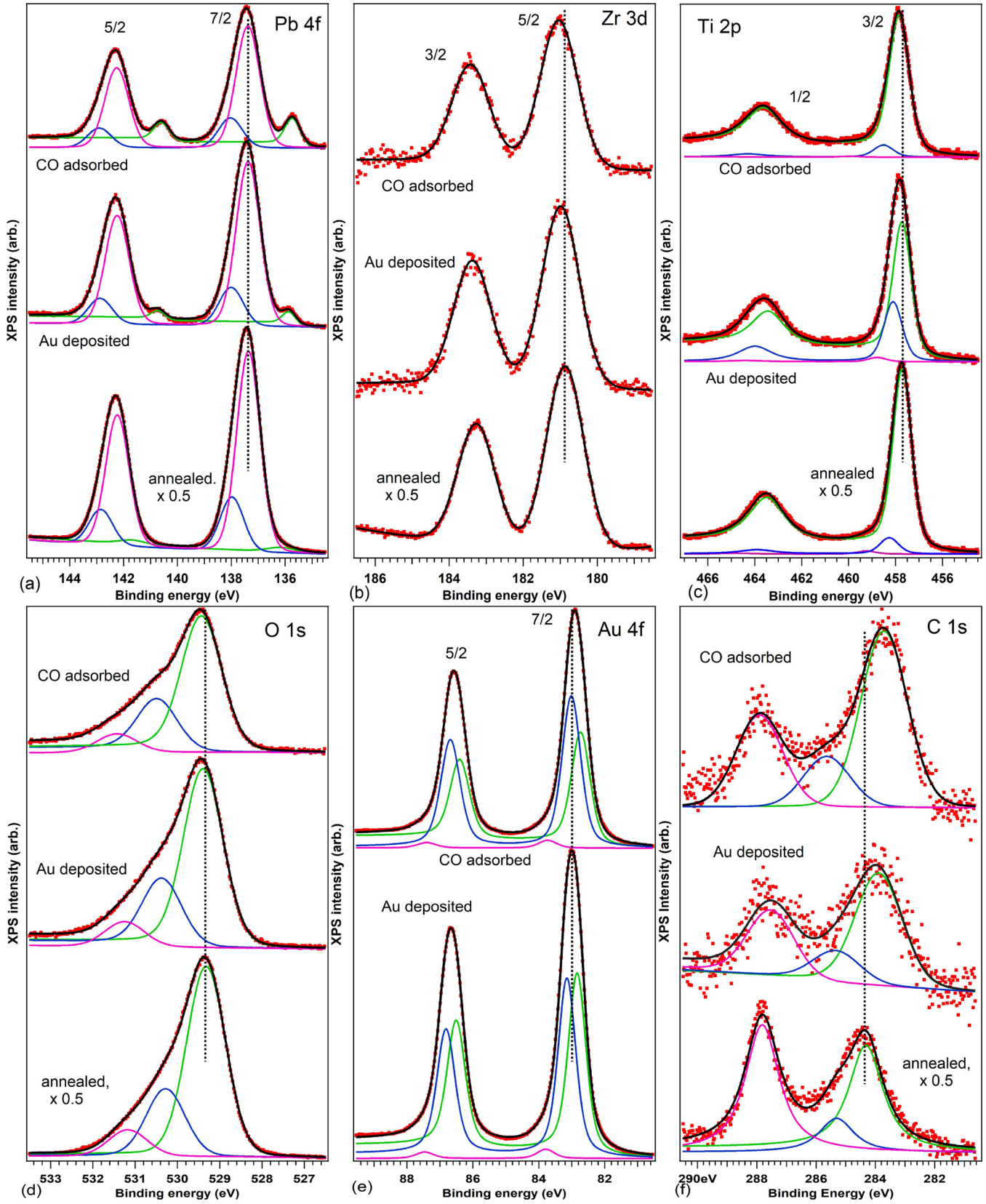

Fig. 1. Soft X-ray photoelectron spectra obtained by using synchrotron radiation on clean PZT(001), after 1 nm equivalent coverage of Au deposited and after 45,000 Langmuir CO adsorbed on this heterosurface: (a) Pb 4f, (b) Zr 3d, (c) Ti 2p, (d) O 1s, (e) Au 4f, (f) C 1s. The employed photon energies were 260 eV for (a,b,e), 400 eV for (f) and 680 eV for (c,d). Spectra are deconvoluted with Voigt singlets (d,f) or doublets (a,b,c,e) with controlled amplitude (branching) ratios, widths and spin-orbit splittings.

AFM determinations are performed in air, in tapping mode after the *in situ* experiment, by using a MFP-3D Asylum Research setup.

3. Results and discussion

3.1. Sample characterization

Fig. 1 presents Pb 4f (a), Zr 3d (b), Ti 2p (c), O 1s (d), Au 4f (e), and C 1s (f) core levels (CLs) recorded with high resolution using the Elettra synchrotron radiation beam, at several stages of the sample history. The spectra for *as introduced* samples were omitted from these representation, since they show a huge contamination C 1s peak and their surface stoichiometry severely differs from that of bulk PZT. All XPS spectra are 'deconvoluted' by using Voigt lineshapes or doublets [40,41], with controllable physical parameters, such as separate lorentzian or gaussian widths, peak to background ratio, choice of similar or dissimilar widths in the case of doublets to account for different core hole lifetimes in the same doublet, when additional core hole decay might occur in the state with lower angular momentum [42], *etc.* The intensity variation of the synchrotron beam with photon energy is known; in addition, a comparison was made with peak intensity ratios obtained by conventional XPS using Al K_α radiation, and in particular the Zr:Ti ratio was strictly checked at each level, since for all previous experiments on similar samples this was never found to differ considerably from 1:4. After proper normalization by the theoretical cross sections [43], by the acceptance function of the analyzer and by the synchrotron radiation beam intensity, the derived intensity ratios are listed in Table 1.

Quite often, the PZT(001) is not stable with respect to the release of neutral (metallic) Pb under intense synchrotron radiation beam [34,35]. This was observed also for the present data, but only after the Au deposition (Fig. 1(a)). The PZT(001) surface after cleaning is quite stable in the synchrotron radiation beam. The same was observed also in Ref. 7. In the actual case, the Pb 4f spectrum for the clean sample does not exhibit the low binding energy (BE) peak at 135.7–135.8 eV (Pb $4f_{7/2}$), it is deconvoluted with a main component at 137.63 eV and a higher BE component at 138.24 eV. This is a sign of a inwards polarized state ($P^{(-)}$) [7,13,16], and the high BE component represents Pb^{2+} with lower oxygen coordination. In Ref. 35 the instability of microscopic areas without out-of-plane polarization ($P^{(0)}$) was connected to a lower value of the dissociation energy of surface PbO– with respect to the maximum kinetic energy of a 'hot electron' in the conduction band, i. e. the electron affinity. The stability of areas with outwards polarization $P^{(+)}$ is related to the fact that even an electron with the highest kinetic energy in the conduction band is unable to produce surface dissociation of PbO, since the dissociation energy of PbO is larger than the electron affinity. Now we have to sketch an explanation for the stability of Pb–O bonds in inwards polarized states. Here one must compare the electron affinity with the dissociation energy of PbO^{2-}, and for sure it should be larger. However, inside the film the bands are bent such as to follow the near surface depolarization field, oriented outwards [44]. Thus, secondary and Auger electrons produced inside the film will be repelled by the surface towards the bulk (Fig. 2 (b)). Even if these 'hot electrons' had initially enough kinetic energy to produce surface dissociation, when reaching the surface their kinetic energy decreases by an amount equal to the band bending (on the order of 1 eV for $P^{(+)}$–PZT [7,13,33,44]) and the remaining kinetic energy does not suffice to produce surface dissociation.

Dissociation with release of metal Pb is quite visible immediately after depositing Au on this surface, according to the Pb 4f spectra of Fig. 1(a). The amount of metal Pb released at the surface increases after exposure to carbon monoxide. Several hypotheses may be formulated to account for these facts. Firstly, when a metal is interfaced with a semiconducting ferroelectric with out-of-plane polarization, extrinsic screening is likely to occur, such that the compensating charges will be located in the metal and thus no band bending (related to the formation of a compensating charge sheet inside the ferroelectric) occurs in the semiconductor, see Fig. 2. Only some small band bending due to metal-semiconductor Schottky effect may subsist, but in the actual case the work function of Au is similar to that of PZT [33], therefore such effect will be neglected. Then, 'hot electrons' produced inside the PZT(001) film would have sufficient energy at the surface to promote dissociation. Secondly: 'hot electrons' with kinetic energies larger than the electron affinity (termed also 'secondary electrons'), for a clean surface, even if provided with enough energy to produce dissociation, escape rapidly from the crystal [35]. In the presence of a metal deposited on top, these secondary electrons are scattered towards the film and the probability of dissociation increases. One may even imagine a 'quantum well' at the interface between the metal and the ferroelectric with inwards polarization, where 'hot electrons' may be stabilized enough time to produce dissociation. Similar considerations may be valid also for contaminating layers, and indeed most experiments on *as introduced* samples using synchrotron radiation pointed out the immediate (within a few minutes or tens of minutes) dissociation of the surface. Thus, the stabilization of ad-molecules (dissociated or not, see later) works in a similar sense towards the release of metal Pb from the surface.

The Zr 3d spectra (Fig. 1(b)) are deconvoluted with only one spin-orbit split doublet, whose BE again (180.9–181.0 eV) points also to a band bending upwards (lower BE), thus to a $P^{(-)}$ polarization state [7]. The Ti 2p spectra (Fig. 1(c)) are simulated with two spin-orbit split doublets, with a higher BE component of lower intensity. The BE of the main component (around 457.7 eV) is also in good agreement with $P^{(-)}$ [7]. The higher BE component could be interpreted as a surface component, and, for the spectrum after Au deposition, its relative intensity increases, which could be a sign of areas with no band bending, where the compensating charges are ensured by the metal particles (Fig. 2(a)). One may question why similar components are not detected in the Zr 3d spectra (Fig. 1(b)). One practical answer for this is related to our general fitting strategy which consist in using always the minimal number of components. Small parasitic components could be introduced in the analysis of the Zr 3d spectra, but the lower statistics of these spectra does not ensure the unique determination of such small components. The O 1s spectra are simulated with three components; in order to retrieve a good stoichiometry (see Table 1) only the lower BE component (529.3–529.4 eV) has to be taken into account. The other two components with BEs of 530.3–530.5 eV and 531.2–531.4 eV may be related most probably to surface oxygen (or hydroxyls) and to C—O bonds [26,45]. Such components are also visible in clean $P^{(-)}$ polarized PZT(001) samples [7]. Note that there is still a C 1s signal after annealing in oxygen (Fig. 1(f)), as will be commented below. The origin of this residual carbon contamination after the cleaning procedure (reduced by a factor or about 50 with respect to the initial contamination) stems in the CO uptake from the residual gas in the UHV chambers. Note that in Ref. 7 the samples were cleaned in the analysis chamber and measured immediately, whereas in the actual case cleaning in oxygen was achieved in a separate chamber, and Au deposition was performed in another chamber. As a consequence, related also to the need of cooling down the sample holder before transferring it, at least

Table 1
Atomic intensity ratios obtained from core levels represented in Fig. 1, after normalization by the beam intensity and by the atomic photoemission cross sections. The normalization to the beam intensity is the main source of the error bars specified in parentheses in the first row.

Atomic ratio Sample	Pb/(Zr + Ti) (± 0.10)	Zr/(Zr + Ti) (± 0.008)	O/(Zr + Ti) (± 0.12)	Au/Pb (± 0.02)	C/Pb (± 0.05)
annealed PZT(001)	2.58	0.200	3.56	–	0.254
1 nm Au deposited	1.52	0.206	3.52	2.95	0.347
45 kL CO dosed	1.39	0.200	3.32	2.98	0.712

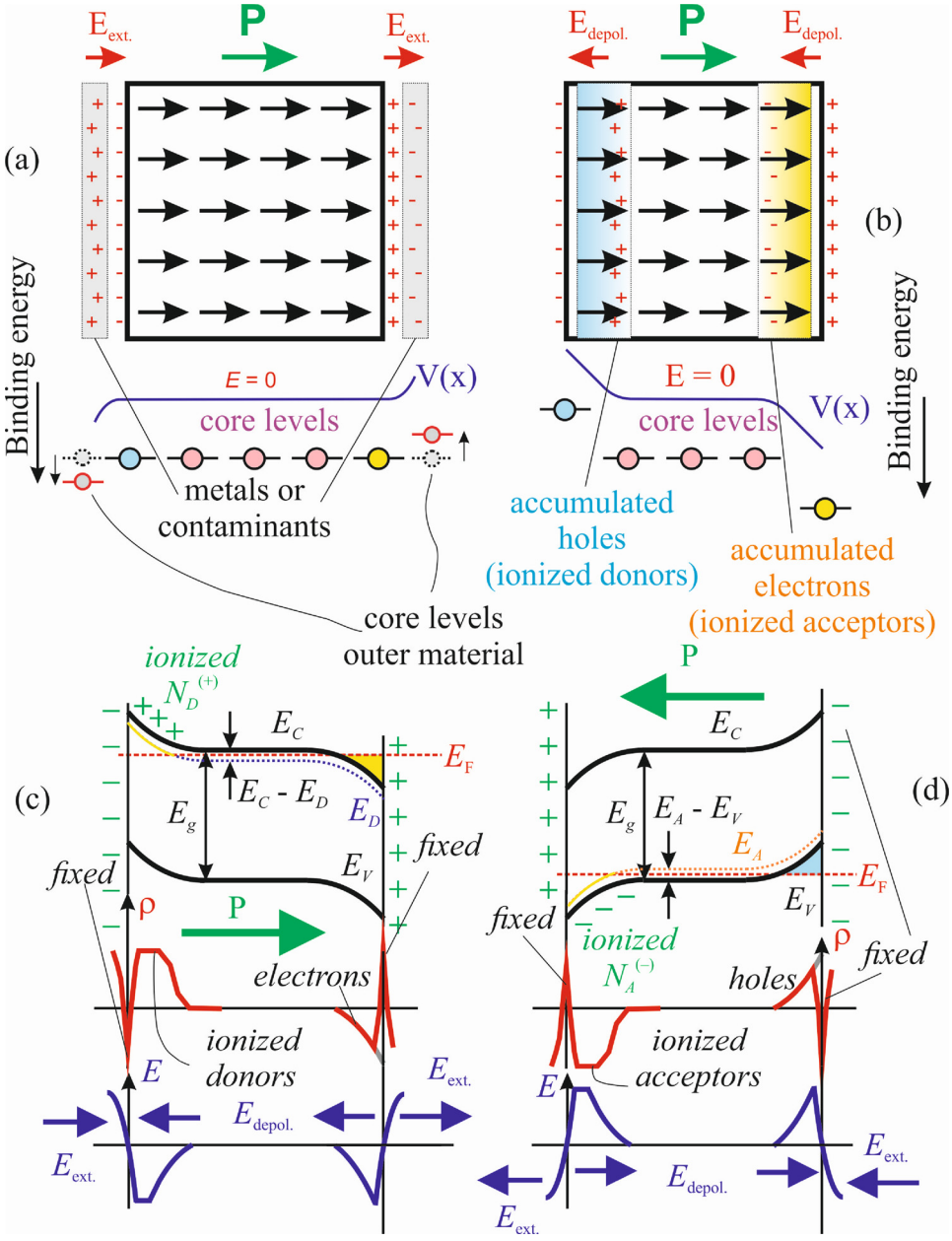

Fig. 2. Schematics of the compensation mechanisms of the depolarization field in a single-domain ferroelectric thin film: (a) extrinsic compensation by (image) charges generated in the metal contacts or in the contaminating layers of sign opposite to the fixed charges at the extremities of the ferroelectric film; (b) intrinsic compensation by charges accumulated *inside* the ferroelectric film, which can be mobile charge carriers and/or ionized impurities; in this case, the surface band bending inside the ferroelectric film is reflected by shifts in the core levels of the material; (c) the case of a strongly n-type doped film, with accumulation of electrons towards the face with outwards polarization and of positively ionized donors towards the face with inwards polarization; (d) the case of s strongly p-type doped film, with accumulation of holes near the face with inwards polarization and of negatively ionized acceptors near the face with outwards polarization. Adapted from Refs. [16] and [44].

one hour is elapsed from the cleaning up to the start of the measurements, including the transfer of the samples through 3 or 4 different chambers. During this waiting and transferring time, the sample uptakes CO from the residual gas, whose total dose, for a partial pressure of 10^{-10} Torr and for 3000–4000 s, is still in the range of a few Langmuir.

Hence, the stoichiometry of the sample is computed by taking into account only the lower BE component of O 1s, the total intensity for Zr 3d and Ti 2p, and all components from Pb 4f except the component representing the metal Pb, when it was visible. The intensity ratios are quite similar to those from Ref. [7]; note that photoelectron diffraction effects could induce deviations from the ideal stoichiometry for a single crystal film [46]. The fact that the O/(Zr + Ti) ratio exceeds 3 may also be related to a p-type self-doping (cation vacancies acting as hole generators), according to the general mechanism of self-doping discussed for n-type doping in Ref. 39 and to the detailed mechanism of induction of the $P^{(-)}$ polarization state commented in Ref. 44 for PZT/SRO(001). Also, the fact that Pb/(Zr + Ti) exceeds 1 is related to the PbO termination of the PZT(001) combined with the surface sensitivity of this technique [[7,33], the effective inelastic mean free path $\lambda \cos \theta$ being close to 1.5 times the *c* (out of plane) lattice parameter of the film (about 4.1 Å [47]). Later on, we will consider as an "effective contribution" to the photoemitted intensity that of 1.5 bulk unit cells.

Surprisingly low BE values are derived for Au 4f, which is simulated with two main components at 82.7–82.8 eV and at 83.0–83.1 eV (Fig. 1(e)). These Au $4f_{7/2}$ BEs are considerably lower than the 'standard' metal Au $4f_{7/2}$ BE at 83.81 eV [48]. In the NIST XPS database there is no such low value for Au $4f_{7/2}$ BE (below 83.2 eV).Only the smallest component at the highest BE approaches the value for metal Au. The interpretations for such low BE is that Au nanoparticles are *negatively charged* or are insulated on areas with inwards polarization $P^{(-)}$, where the upwards band bending originating from the ferroelectric is transferred to the energy levels from gold. Negatively charged gold was detected in an early experiment with Au deposition on PZT(001), though not cleaned prior to the Au deposition [33]. But in the actual case most gold is found in the negative charge state. As a rough estimate, taking into account that Au^{3+} (from Au_2O_3) is found at 2.1 eV higher BE [49], and taking into account also the surface band bending

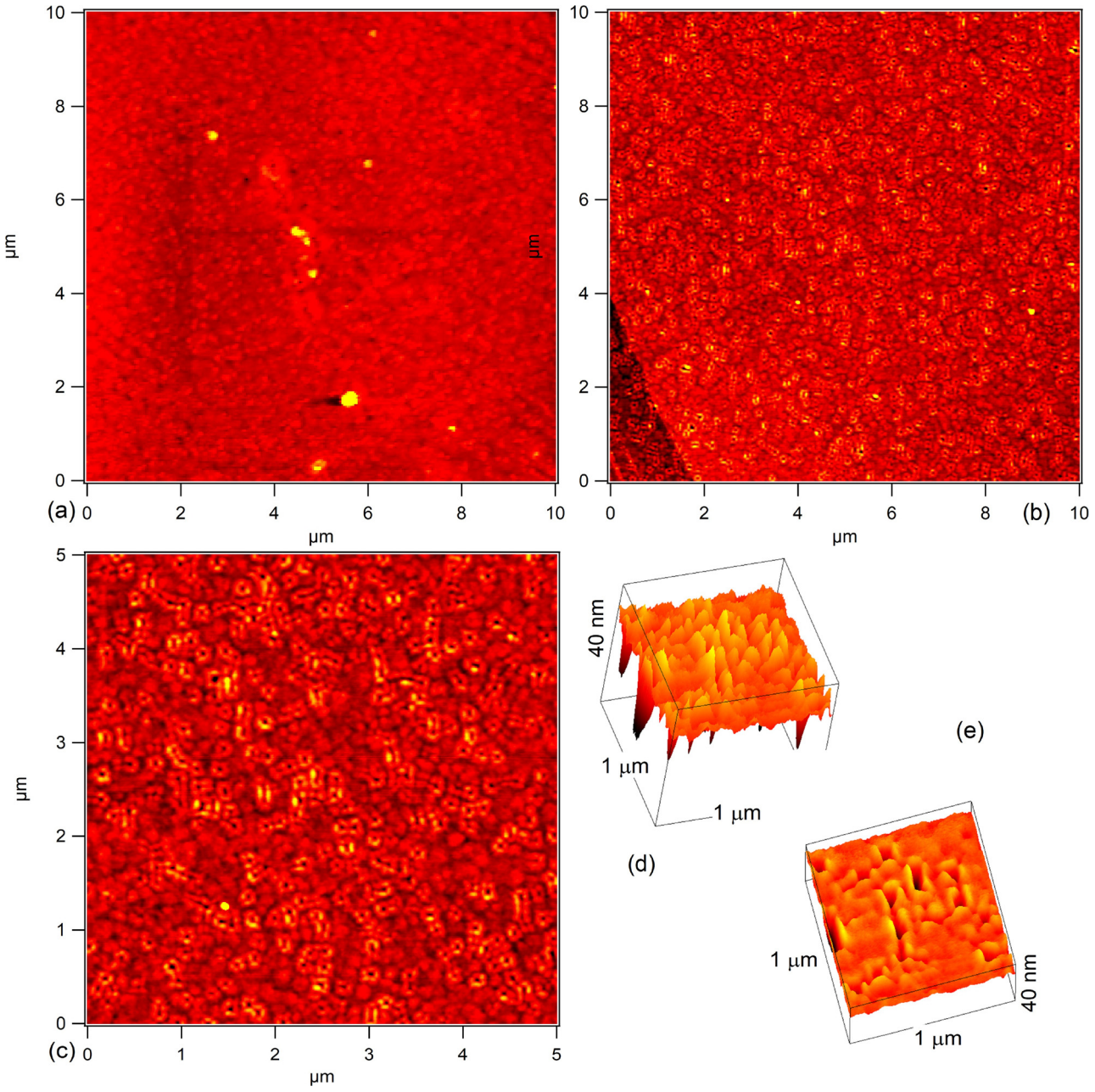

Fig. 3. Atomic force microscopy images obtained in air on Au/PZT(001) surfaces after their preparation by PLD (a) and after cleaning in UHV followed by Au deposition, CO adsorption and synchrotron radiation experiment (b–e). Areas investigated: (a, b) 10 × 10 μ m^2, (c) 5 × 5 μ m^2. (d, e) 3D plots of a 1 × 1 μ m^2 area, to reveal the size and shape of Au nanoparticles. RMS roughness: 1.08 nm for (a), 1.34 nm for (b), 1.44 nm for (c) and 3.46 nm for (d, e).

towards lower BE of about 1 eV, it looks as each gold atom carries almost a *–e* charge. Thus, such heterosurfaces are expected to show enhanced chemical activity [37].

Indeed, after exposure to a saturating dose of CO, the C/Pb ratio exceeds 0.7, according to Table 1. Also, as in Ref. 7, a significant amount of carbon is found in reduced (graphitic) state with the C 1s BE at 283.6–283.7 eV, which is the value used for 'adventitious carbon' found in most XPS spectra (284.6–284.7 eV) affected by the surface band bending of about 1 eV. Two other C 1s components are detected at 285.3–285.6 eV and at 287.7–287.9 eV. The easiest attribution of these components are carbon bound to oxygen by single or double bonds, respectively [45]. The graphitic carbon represents about 58 % of the total amount of carbon, C—O about 16 % and C═O about 26 %. Hence, the ratio between reduced carbon and lead (C(r)/Pb) from PZT saturates at about 41 %, value, quite close to the value reported in Ref. 7 immediately after dosing CO. However, in the above Ref. most carbon is desorbed in a few tens of seconds, and one reaches a C(r)/Pb ratio of 0.29 before the heating experiment started. As compared with the previous data on clean, inwards polarized PZT(001) without gold deposition, it seems that in the actual case, although the saturation coverage is similar just after dosing, the sticking of carbon-related molecules is much more robust with respect to photoinduced desorption. The above C/Pb ratio will be in the following normalized to the "effective contribution" represented by about 1.5 formula units. A ratio of 0.71 for C/Pb is translated then in 0.47 monolayers (ML), by ML meaning the coverage obtained by attributing to each surface elementary cell a carbon atom (about 6.5 × 10^{19} m^{-2} surface density). Note also that 0.75 monolayers (ML) seems to be some kind of 'universal' saturation coverage of carbon monoxide on noble metals [50]; ethanol or carbon dioxide saturation coverage is even lower (in the range of

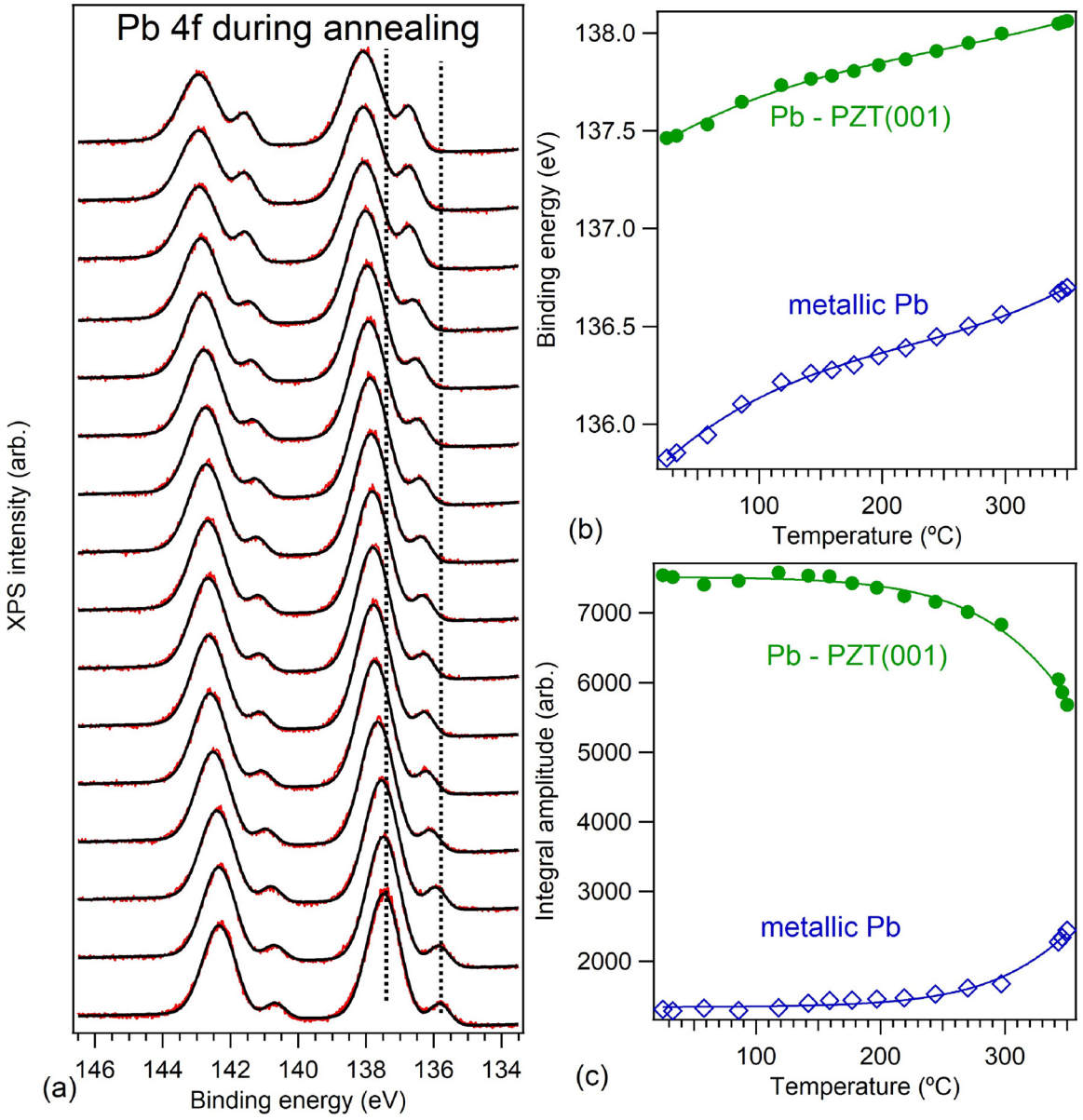

Fig. 4. Pb 4f time and temperature-resolved photoelectron spectroscopy data: (a) Pb 4f spectra, after CO adsorption on Au@PZT(001); red lines are raw data, black lines are fits using Gaussian doublets with a minimal number of coefficients; (b) variation of binding energies of different components with sample temperature; (c) temperature variation of amplitudes of the three different components. Photon energy employed: 400 eV (For interpretation of the references to colour in this figure legend, the reader is referred to the web version of this article).

0.1–0.2 ML) on ferroelectric $BaTiO_3$ [21]. Thus, the derived saturation coverage of 0.7 C(r)/Pb, or 0.47 ML, which means nearly one C atom for two PbO surface cells, is a promising result at room temperature.

Moreover, if one compares with the results obtained on clean PZT(001) [7], one may notice that the amount of oxidized carbon were about 29 % in that work, being the equivalent of about 0.08 ML, while about 0.2 ML of the carbon atoms are in the graphitic state (dissociated). (The values from Ref. 7 were also divided by 1.5, which corresponds to the inelastic mean free path in terms of effective Pb atoms visible by photoemission. The photon energies used in both experiments were the same.). In the actual case, from the total amount of 0.47 ML, 0.27 ML is found in the reduced (graphitic) state and 0.2 ML in oxidized state; moreover, two different oxidation states are detected. It looks like the presence of gold nanoparticles on the surface enhances more favorably the amount of molecular carbon (0.12 ML of additional carbon adsorbed additionally in oxidized states to be compared with 0.07 additional carbon in reduced state.) The additional amount of reduced carbon could also be attributed to a stronger polarization of the sample used in this work. This sample, with 50 nm thickness, exhibits a surface band bending of nearly 1 eV, whereas the 20 nm PZT(001), used in Ref. 7, showed a surface band bending of 0.6–0.7 eV. Thus, a more robust polarization might enhance the reductive properties of this surface [12,14]. Au nanoparticles, especially in a relative negative state, might have a beneficial effect on the back-donation mechanism [30] when CO molecules interact with the surface of a negatively charged Au nanoparticle.

It follows that an important point is to evaluate the surface morphology and the amount of the surface covered by Au nanoparticles. Fig. 3 presents AFM scans on the sample surface, performed after *in situ* CO adsorption-desorption experiments. Structures resembling 'fortifications' with walls of 2 nm together with 'towers' of 4–6 nm height surrounding 'pools' of about 20 nm depth are identified (Fig. 3(c, d)). The root mean square (RMS) roughness for an extended area (10 × 10 μm^2) is 1.34 nm, while the RMS roughness for a restricted area

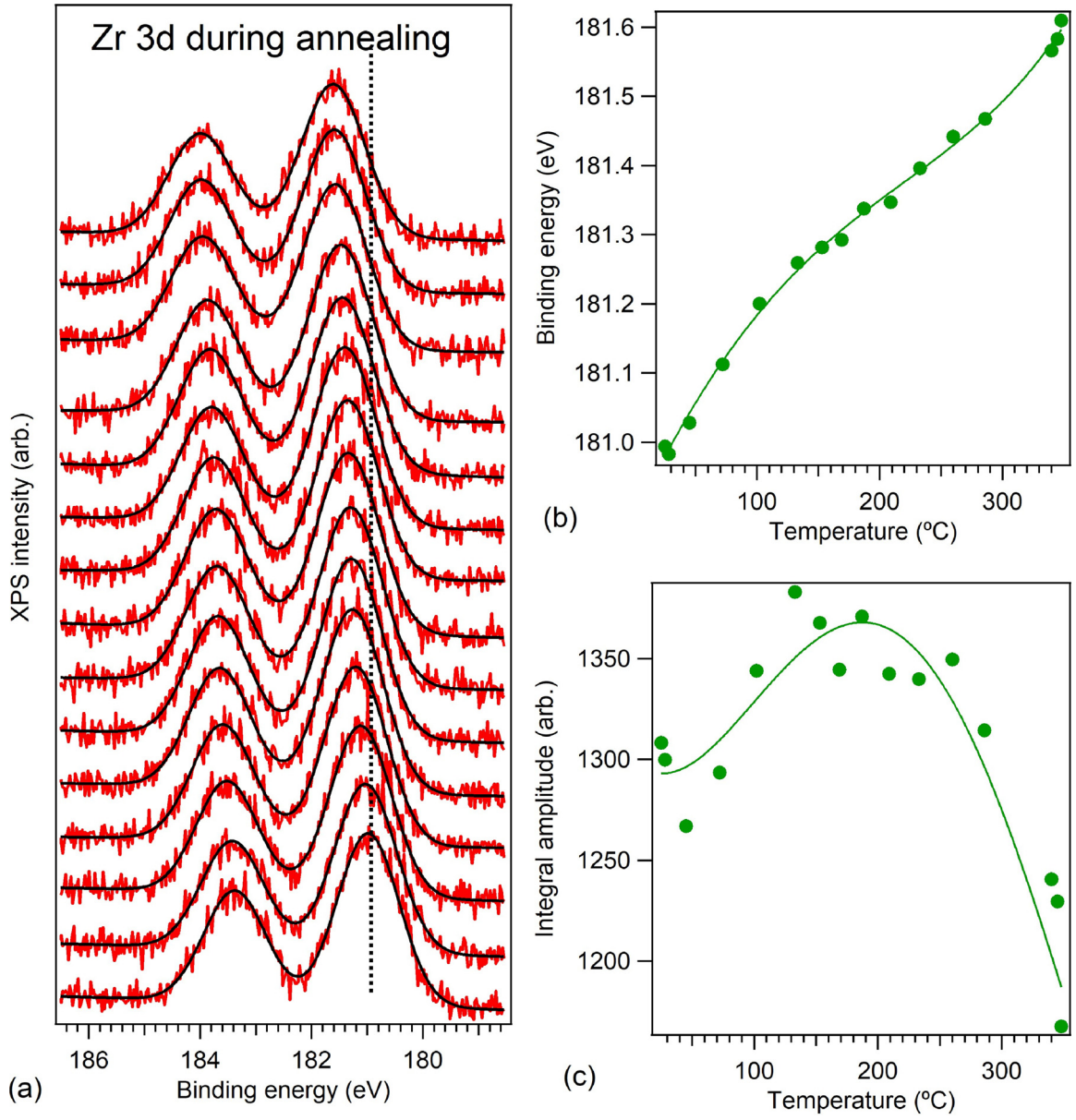

Fig. 5. Zr 3d time and temperature-resolved photoelectrons spectroscopy. Similar observations as for Fig. 4. Photon energy: 400 eV.

containing a significant part of Au nanoparticles exceeds 3 nm (Fig. 3(d, e)). Note that the RMS roughness of the 50 nm PZT(001) sample recorded before Au deposition is of about 1 nm (Fig. 3(a)), and such surfaces are in principle saturated by the naturally attached contaminant molecules [12]. It is then difficult to estimate from such a measurement performed in air the contribution to the surface roughness of the PZT film, of contaminant molecules or of the deposited gold overlayer. However, the significantly larger RMS roughness in areas where we suppose that Au nanoparticles are formed is in line with the amount of gold deposited, 1 nm if the film was completely flat. The lateral size of these structures varies between 50 and 100 nm, and they occupy roughly one half of the surface, which is in line with the 'effective' gold coverage of 1 nm deposited. The origin of the 'pools' is probably connected to the substrate disruption and consumption of Pb. It might be possible that 'consumed' Pb mixes with Au to build up the walls of the 'fortifications'. Indeed, Pb with Au forms solid solutions over the whole range of compositions, with well-defined intermediate compounds Au_2Pb, $AuPb_2$ and $AuPb_3$ [51].

3.2. Follow-up of in situ desorption of carbon monoxide

In addition to the need to present in which measure the adsorbed carbon is related to the polarization of PZT and also to investigate the way to regenerate the catalytic heterosurface, this study will help us to identify the nature of different components in C 1s and Au 4f and also to assess to what extent Au atoms found at lower binding energies are negatively ionized or just shifted by the surface band bending of the PZT. Also, one needs to investigate the stability of the ferroelectric surface with respect to metal Pb release.

Figs. 4–9 present time-resolved scans (Fig. 4 for Pb 4f, Fig. 5 for Zr 3d, Fig. 6 for Ti 2p, Fig. 7 for O 1s, Fig. 8 for C 1s and Fig. 9 for Au 4f) recorded while heating the surface with 45 kL CO dosed on it. The photon energy was different for practical reasons connected to the need of rapid scans: 400 eV for Pb 4f, Zr 3d, Au 4f and C 1s; and 680 eV for Ti 2p and O 1s. The spectra are deconvoluted with Gaussian lineshapes with associated inelastic backgrounds (erf), with the exception of Ti 2p and O 1s where, due to the larger core hole width (0.22 and 0.24 eV for Ti $2p_{3/2}$ and $2p_{1/2}$, respectively [52], and about 0.18 eV for O 1s [53]) Voigt profiles were preferred.

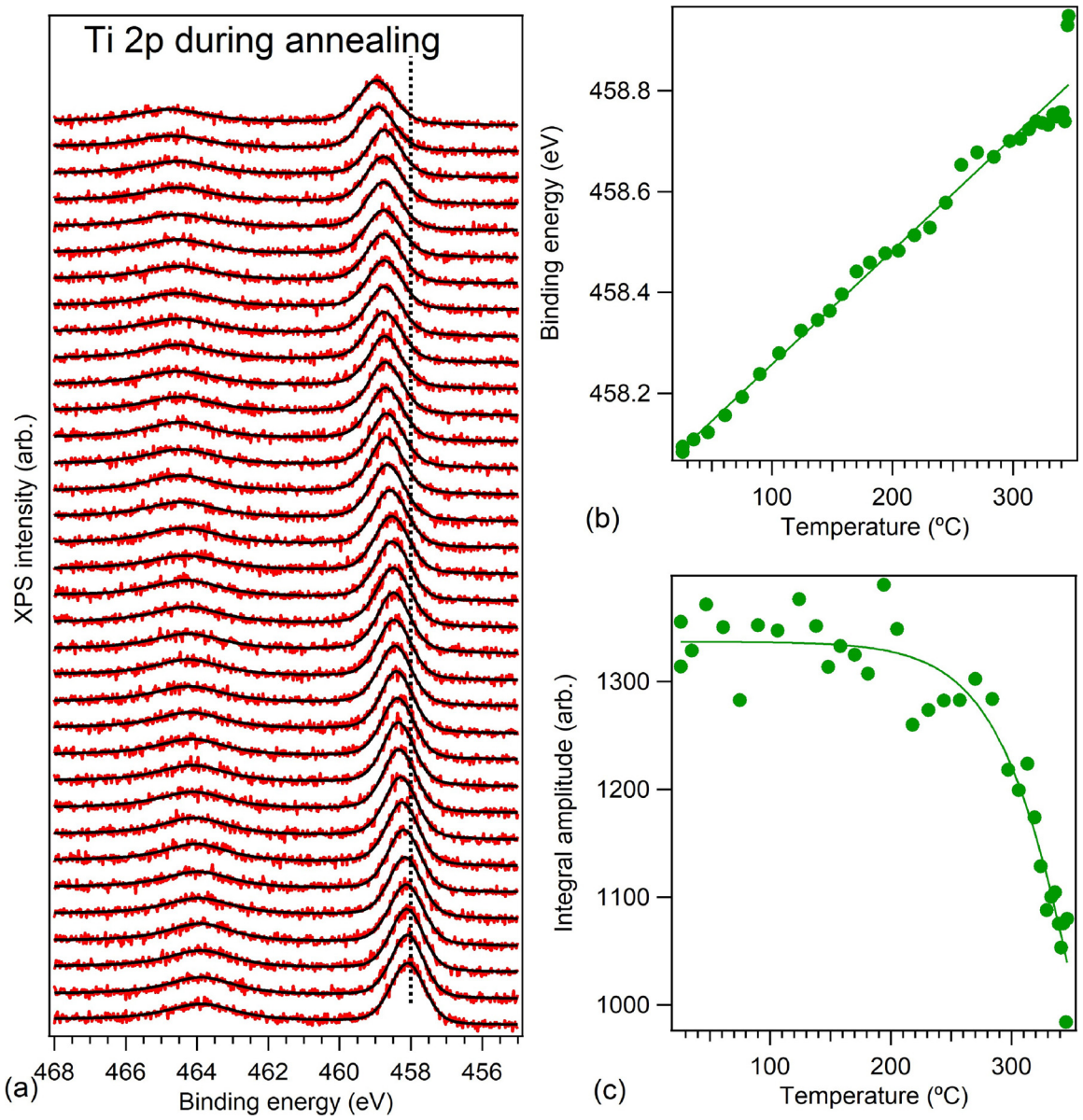

Fig. 6. Ti 2p time and temperature-resolved photoelectrons spectroscopy. Similar observations as for Figs. 4 and 5, with the only difference that in this case, the spectra are simulated with Voigt doublets. Photon energy: 680 eV.

All CLs from the substrate vary towards higher BE when the sample is heated: 0.60 eV for Pb 4f from PZT(001), 0.62 eV for Zr 3d, 0.87 eV for Ti 2p, 0.94 eV for O 1s from PZT(001), 0.84 eV for the largest component of Au 4f and 0.27 eV for C 1s for carbon in reduced form. This is a sign of the progressive loss of the inwards polarized state when the sample is heated, as in Ref. [7]. Also, the variation is larger for Ti 2p and O 1s owing probably to a larger participation of their valence orbitals (O 2p and Ti 3d) to the charge accumulation or depletion near surface. For Au 4f, the main component upon heating approaches the BE of neutral bulk Au (83.78 eV). Also, all CL intensities decrease progressively with the increase of the temperature, which can be attributed to the progressive misalignment of the photoelectron detection setup, namely to the position of the sample excited by the small spot soft X-ray beam ($10 \times 100\ \mu m^2$) in the focus of the analyzer. But not only, as will be commented below.

The Pb 4f evolution (Fig. 4) exhibits a progressive increase of the metal Pb contribution with simultaneous decrease of the contribution of Pb from PZT(001), starting with temperatures above ~ 250 °C. According to the evolution of CL BEs, this implies that substrate disruption occurs nearly the temperature where the ferroelectric polarization decreased significantly. This is in line with the remarks from the previous Section and from the findings detailed in Ref. 32, that demonstrate how unpolarized PZT(001) is unstable with respect to surface photodissociation. According to the observations by AFM, metal Pb is precipitated near the areas already occupied by Au nanoparticles. One direct consequence for the data analysis is that, in these conditions, one should expect a stronger decrease of all the other CL intensities coming from unaffected PZT(001). Firstly, the area free from (Au + Pb) nanoparticles is expected to decrease, then in these areas occupied by nanoparticles the CLs from the substrate are attenuated due to the photoelectron inelastic mean free paths. Indeed, this is the case for Zr 3d (Fig. 5), Ti 2p (Fig. 6) and O 1s (Fig. 7). This also makes it difficult the evaluation of C(r)/Pb(PZT) ratio as a measure of carbon release from the surface at increasing temperature. Conversely, such evaluation can still be performed before the onset of the additional metal Pb. In particular, the Ti 2p and O 1s intensities are almost constant before the onset of metal Pb. We do not have an explanation for the small increase of the Zr 3d intensity in the intermediate temperature range (100–200

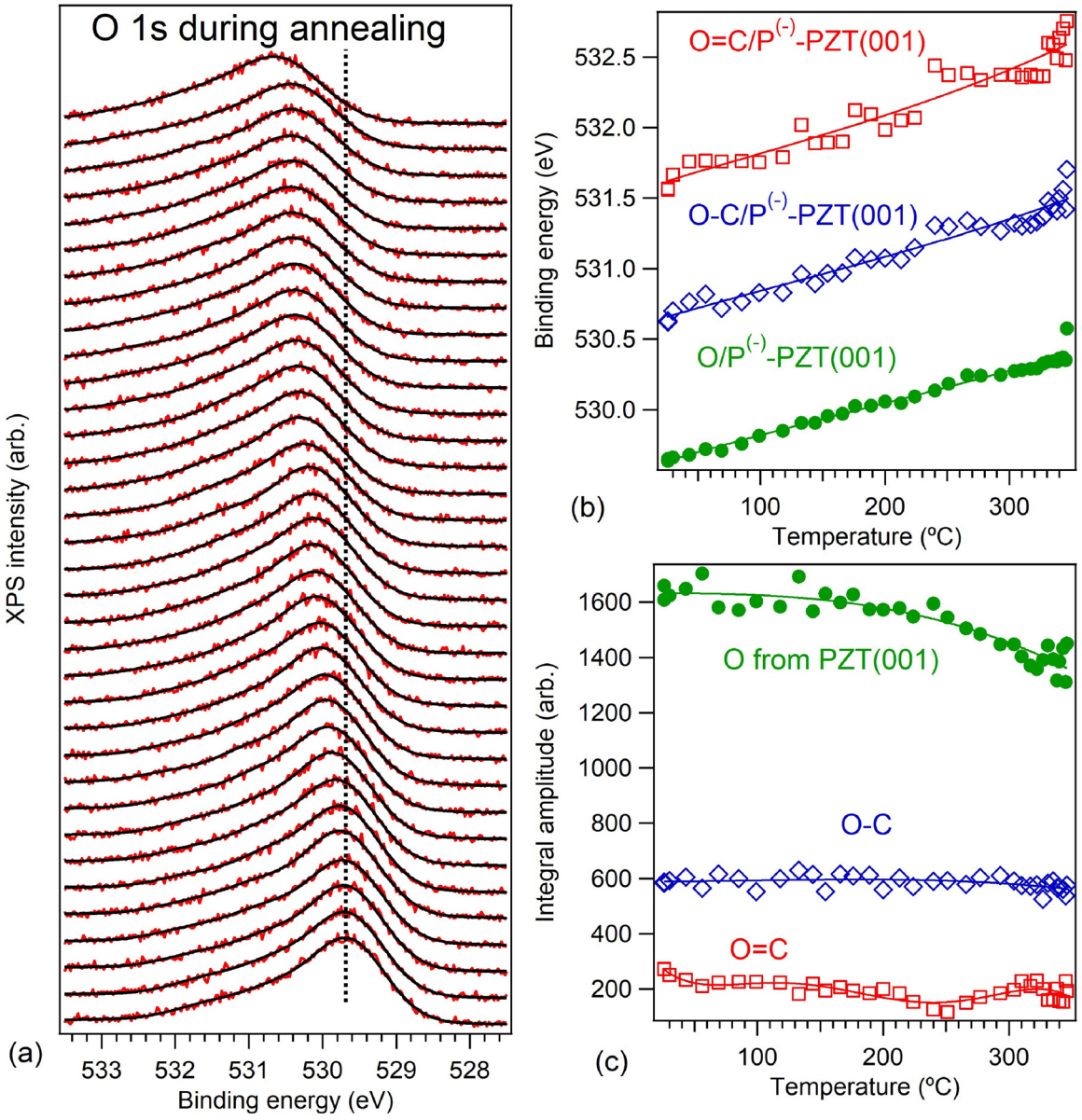

Fig. 7. O 1s time and temperature-resolved photoelectrons spectroscopy. Similar observations as for Figs. 4 and 5, with the only difference that in this case, the spectra are simulated with Voigt singlets. Photon energy: 680 eV.

˚C). Also, let us remark that the oxygen components attributed to chemical bonds involving carbon (blue and red curves from Fig. 7(c)) are almost constant. Almost constant with the temperature are also C 1s component of higher BEs, attributed to oxidized carbon (Fig. 8(c)).

As stated above, the evolution of the main component for Au 4f evolves towards the BE of metal Au, while the other two components evolve towards 84.63 eV and 82.68 eV when the polarization-induced band bending decreases. The first (blue in Fig. 9(b,c)) component is Au most probably bound to carbon monoxide, and the second still represents negatively charged Au. As compared with the data commented in the previous Section (Fig. 1(e)), the relative intensity of negatively charged gold decreases considerably. Note that the Au 4f from Fig. 1(e) was recorded with a photon energy of 260 eV, while the data from Fig. 9 were recorded with photon energy 400 eV, therefore with lower surface sensitivity. One can then infer that negatively charged gold may be found at the surface of the gold nanoparticles. Also, it might happen that these areas are progressively 'discharged' by photoemission. These two phenomena may justify a considerably lower proportion of negative gold, but it is still present on the sample in the temperature induced desorption scan.

These observations are synthesized in Fig. 10, where the carbon coverage derived from all core level evolution (in fact, from the interpolated curves) is represented as function of the Pb $4f_{7/2}$ binding energy, hence on the average value of the inwards polarization. The fact that negatively charged gold is found mostly at the outer surface of gold nanoparticles may be corroborated with the extrinsic compensation mechanism implying the creation of positive charges in gold at the interface with the ferroelectric substrate. Also, the fact that most neutral carbon is desorbed when the polarization is lost at higher temperatures together with a lower desorption of oxidized carbon implies (as a rough model) that CO reaching the free ferroelectric substrate are dissociated owing to the strong field in this region, a polarization mechanism which is discussed in more details in Ref. [7]. Briefly, the electric field in the outer region is:

$$\mathcal{E} = \frac{P}{\varepsilon_0} \tag{1}$$

and the molecular polarizability α of CO is written by introducing a

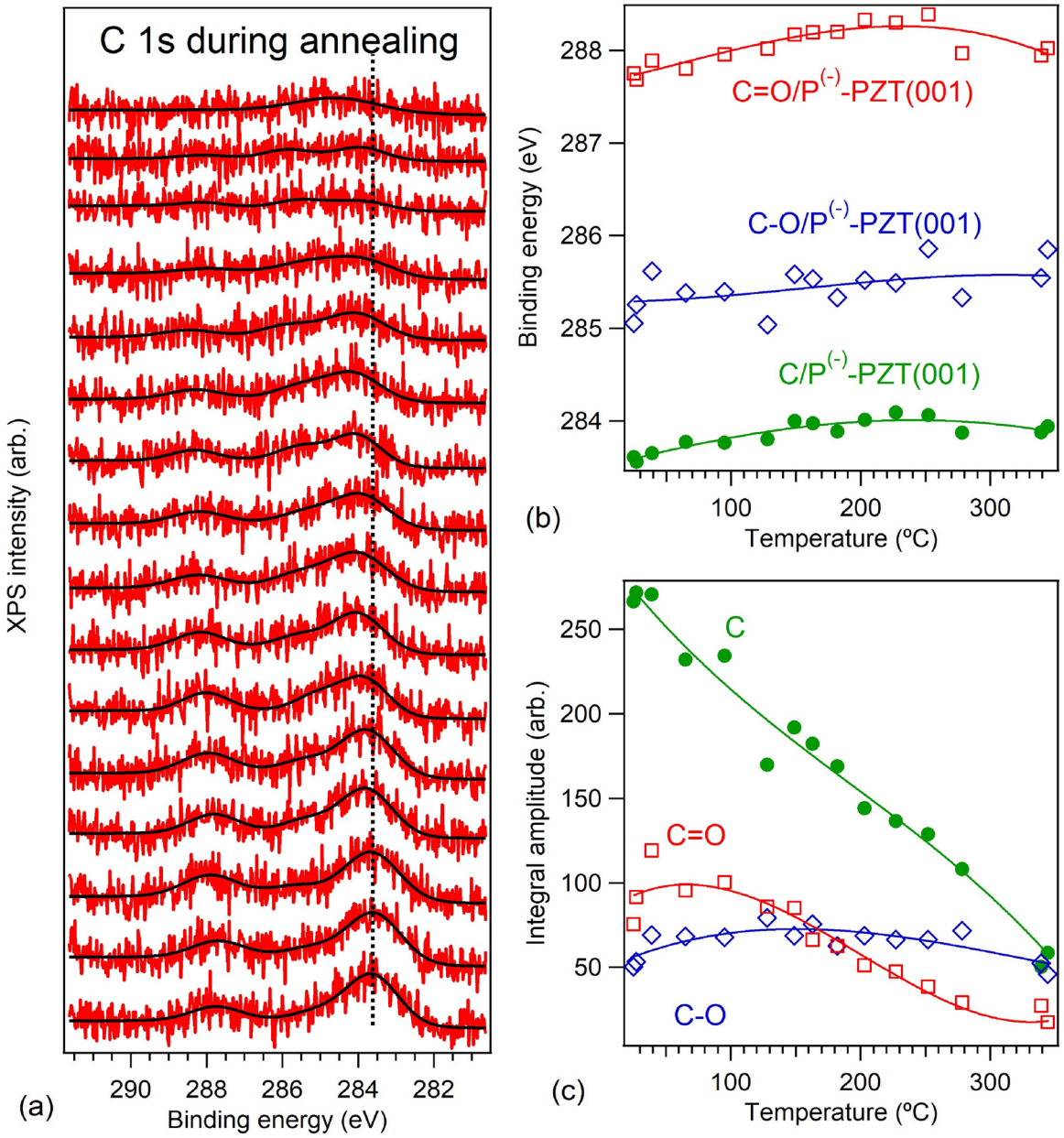

Fig. 8. C 1s time and temperature-resolved photoelectrons spectroscopy. Similar observations as for Figs. 4 and 5, with the only difference that in this case, the spectra are simulated with Gaussian singlets. Photon energy: 400 eV.

'polarization volume' V_p [54]:

$$\alpha = 4\pi\varepsilon_0 V_p \tag{2}$$

One may then estimate the interaction energy between the CO molecule and the external field:

$$W = \int p d\mathcal{E} = \frac{\alpha\mathcal{E}^2}{2} = \frac{2\pi P^2 V_p}{\varepsilon_0} \tag{3}$$

yielding 8.7 eV for $V_p = 1.95$ Å^3 [55] and $P = 1$ Cm^{-2}. This value approaches the dissociation energy of CO (9.6–9.9 eV [56]). For an increase of 10 % in P, the electrostatic interaction energy exceeds the dissociation energy.

Carbon monoxide adsorbed on Au (and then on Au + Pb) nanoparticles seems to be found mostly in an oxidized (bound CO molecules) state and is less sensitive to the polarization decrease of the substrate. It seems that even though the Au 5d t_{2g} orbital positions might have some influence on the π^* backbonding, the fact that the 5d occupancy is the same in neutral or negative gold does not influence in a considerable way the back-donation such as to render the carbon – oxygen bond weaker and eventually to dissociate the molecule. An infrared spectroscopic investigation could offer some more hints on this process and these experiments are planned for the future, when an infrared spectrometer will be attached to the ultrahigh vacuum installation.

Finally, we estimated also the decrease in oxygen content and found a moderate decrease of about 0.05 oxygen atoms per formula unit at 250 °C, when the desorption of neutral carbon was about 0.2 ML (again, according to the definition of one ML, this represents the number of carbon atoms per surface formula unit). Thus, in order to build up CO to be desorbed, the substrate must be depleted by 0.05 oxygens on about 4 unit cells; and to build up CO_2, the oxygen depletion must arrive on 8 unit cells. This is a lower oxygen depletion with respect to Ref. [7]; however, one cannot imagine a mechanism for the desorption of graphitic carbon in ultrahigh vacuum other than the oxygen uptake from the substrate. However, this moderate oxygen depletion was found to be completely recoverable by new treatments in oxygen atmosphere, thus the catalytic heterosurface may be easily regenerated.

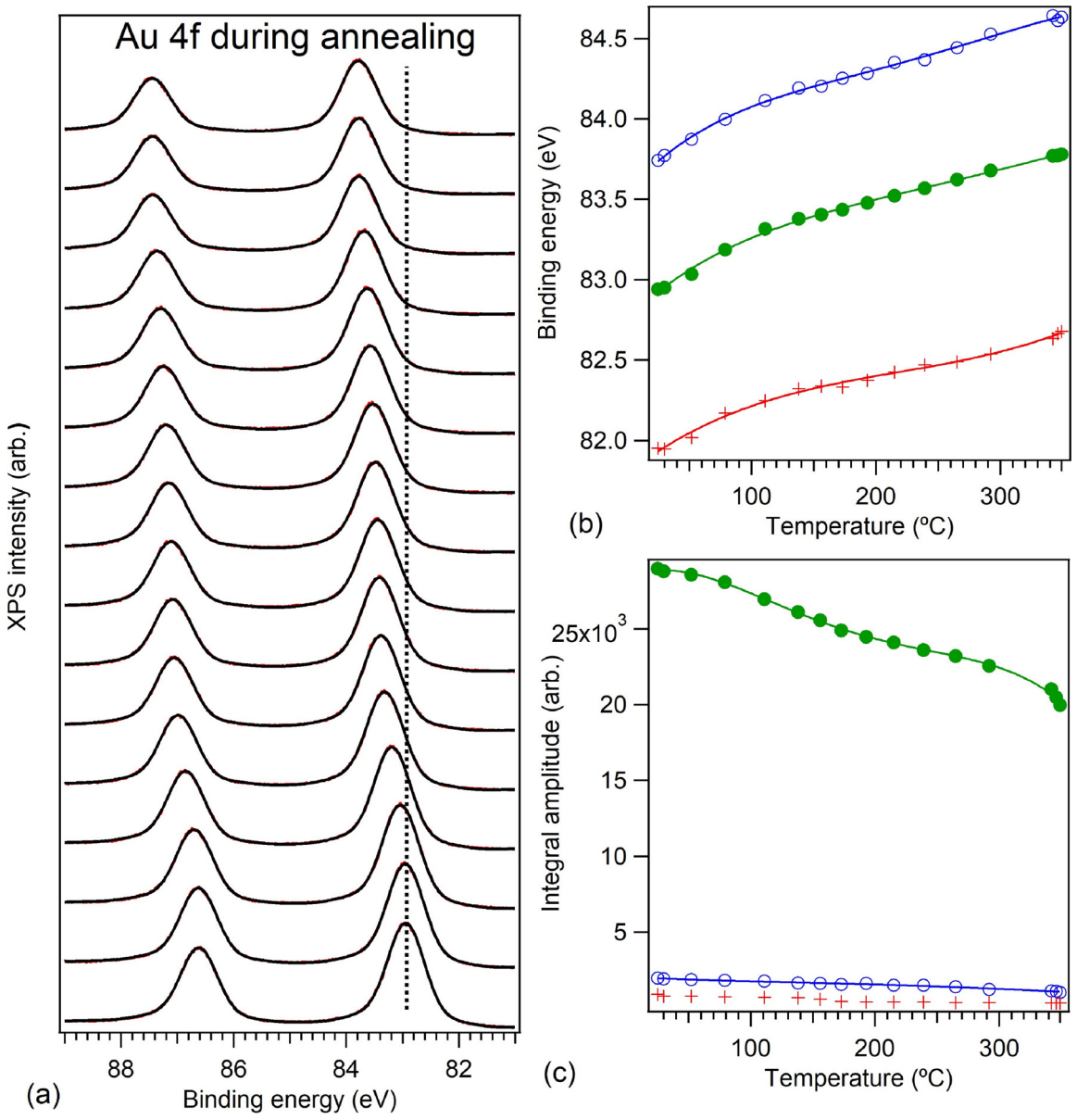

Fig. 9. Au 4f time and temperature-resolved photoelectrons spectroscopy. Similar observations as for Figs. 4 and 5. Photon energy: 400 eV.

4. Conclusions

Associating with gold nanoparticles a clean ferroelectric surface with inwards polarization yielded an enhanced amount of CO adsorption, by about 68 %. Relatively more carbon is adsorbed in molecular state with respect to the case of the ferroelectric surface alone; this was found to be directly connected to the presence of gold nanoparticles. With temperature increase up to the loss of ferroelectric polarization, the amount of molecular CO bound to metal nanoparticles does not decrease significantly, which suggests the independence of the back-donation processes on the ferroelectric state of the surface. Reduced carbon seems to be absorbed mostly on the clean ferroelectric areas alone and is desorbing drastically with the loss of the ferroelectric state at higher temperature, by oxygen uptake from the substrate. A drawback of this kind of heterosurface is that in areas where the ferroelectric surface is lost, it is not stable against release of metal Pb under a flux of about 10^{10} photons/sec/mm^2 (using photons of 260 eV). This happens also in regions where the near surface band bending in the ferroelectric material vanishes due to an extrinsic screening of the depolarization field by the metal nanoparticles. A possible synergistic effect of metal nanoparticles and ferroelectric substrates may be: (i) for the substrate, the stabilization of a larger polarization in the ferroelectric material *via* the extrinsic screening provided by the metal nanoparticles; (ii) for the nanoparticles, the induction of the negative charge state which might influence the carbonyl bonding.

Credit author statement

Nicoleta G. Apostol: Synchrotron radiation experiment, data analysis.

Marius A. Huşanu: Synchrotron radiation experiment.

Daniel Lizzit: Synchrotron radiation experiment, manuscript review.

Ioana A. Hristea: Data analysis.

Cristina F. Chirilă: Ferroelectric thin film preparation.

Lucian Trupină: Sample characterization by AFM.

Cristian M. Teodorescu: Synchrotron radiation experiment, data analysis, manuscript elaboration.

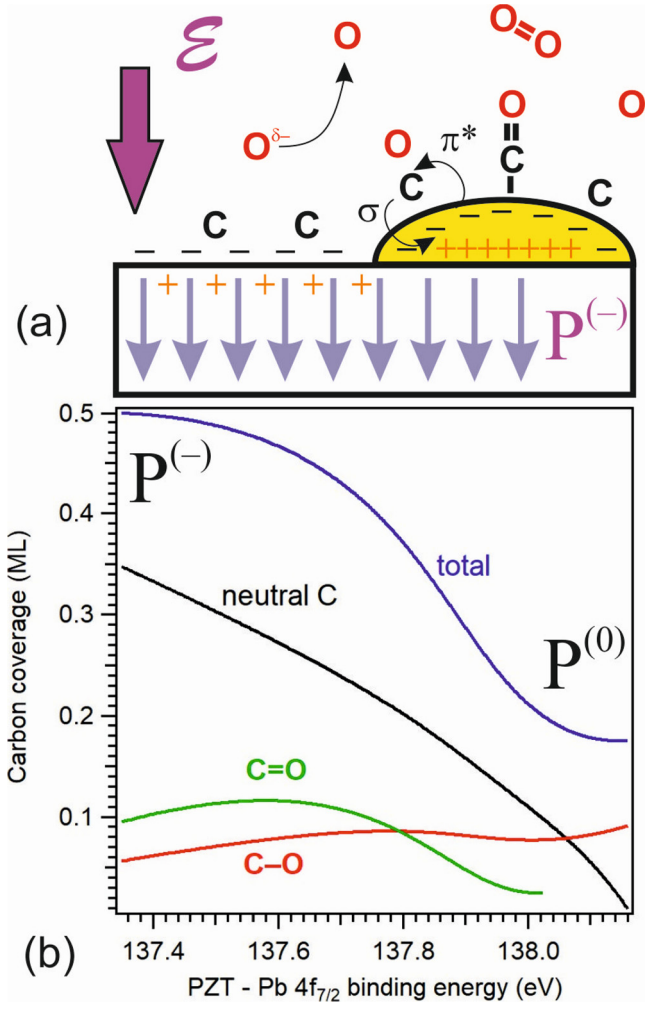

Fig. 10. Schematics of the PZT(001) surface with inwards polarization prone to adsorb dissociated carbon and of a Au nanoparticle with surface negative charge, prone to adsorb molecular CO *via* back-donation processes.

Declaration of Competing Interest

None.

Acknowledgements

This work is funded by the Romanian Ministry of Research and Innovation (RMRI) through the NIMP Core Program PN19-03 (Contract no. 21 N/08.02.2019), PN3–PCCDI Program (Contract No. 75PCCDI/2018) and through the Operational Programme Competitiveness 2014–2020 Program, Project: NANOBIOSURF–SMIS 103,528. N. G. A. is funded by the contract PN-III-P1-1.1-PD-2016-1322, granted by the UEFISCDI agency and acknowledges also a grant attributed by L'Oréal – UNESCO "For Women in Science".

References

[1] K.W. Kolasinski, Surface Science. Foundations of Catalysis and Nanoscience, third edition, Wiley, Chichester, 2012.
[2] A. Kakekhani, S. Ismail-Beigi, Ferroelectric-based catalysis: switchable surface chemistry, ACS Catal. 5 (2015) 4537–4545.
[3] C.Y. Chao, Z.H. Ren, Y.H. Zhu, Z. Xiao, Z.Y. Liu, G. Xu, J.Q. Mai, X. Li, G. Shen, G.R. Han, Self-templated synthesis of single-crystal and single-domain ferroelectric nanoplates, Angew. Chem. Int. Ed. 51 (2012) 9283–9287.
[4] A. Kakekhani, S. Ismail-Beigi, Polarization-driven catalysis via ferroelectric oxide surfaces, Phys. Chem. Chem. Phys. 18 (2016) 19676–19695.
[5] A.M. Kolpak, I. Grindberg, A.M. Rappe, Polarization effects on the surface chemistry of $PbTiO_3$-Supported Pt films, Phys. Rev. Lett. 98 (1–4) (2007) 166101.
[6] S. Kim, M. Rutenberg Schoenberg, A.M. Rappe, Polarization dependence of palladium deposition on ferroelectric lithium niobate (0001) surfaces, Phys. Rev. Lett. 107 (1–4) (2011) 076102.
[7] L.C. Tănase, N.G. Apostol, L.E. Abramiuc, C.A. Tache, L. Hrib, L. Trupină, L. Pintilie, C.M. Teodorescu, Ferroelectric triggering of carbon monoxide adsorption on lead zirco-titanate (001) surfaces, Sci. Rep. 6 (1–18) (2016) 35301.
[8] K. Garrity, A. Kakekhani, A. Kolpak, S. Ismail-Beigi, Ferroelectric surface chemistry: first-principles study of the $PbTiO_3$ surface, Phys. Rev. B 88 (1–11) (2013) 045401.
[9] M.A. Khan, M.A. Nadeem, H. Idriss, Ferroelectric polarization effect on surface chemistry and photo-catalytic activity: a review, Surf. Sci. Rep. 71 (2016) 1–31.
[10] E. Ramos-Moore, J.A. Baier-Saip, A.L. Cabrera, Desorption of carbon dioxide from small potassium niobate particles induced by the particles' ferroelectric transition, Surf. Sci. 600 (2006) 3472–3476.
[11] Y. Yun, L. Kampschulte, M. Li, D. Liao, E.I. Altman, Effect of ferroelectric poling on the adsorption of 2-propanol on $LiNbO_3$(0001), J. Phys. Chem. 111 (2007) 13951–13956.
[12] L.E. Ştoflea, N.G. Apostol, L. Trupină, C.M. Teodorescu, Selective adsorption of contaminants on $Pb(Zr,Ti)O_3$ surfaces shown by X-ray photoelectron spectroscopy, J. Mater. Chem. A Mater. Energy Sustain. 2 (2014) 14386–14392.
[13] C.M. Teodorescu, L. Pintilie, N.G. Apostol, R.M. Costescu, G.A. Lungu, L. Hrib, L. Trupină, L.C. Tănase, I.C. Bucur, A.E. Bocîrnea, Low energy electron diffraction from ferroelectric surfaces. Dead layers and surface dipoles in ultraclean $Pb(Zr,Ti)O_3$(001), Phys. Rev. B 96 (1–15) (2017) 115438.
[14] Y.F. Cui, J. Briscoe, S. Dunn, Effect of ferroelectricity on solar-light-driven photocatalytic activity of $BaTiO_3$ – influence on the carrier separation and Stern layer formation, Chem. Mater. 25 (2013) 4215–4223.
[15] E.S. Beh, S.A. Basun, X.F. Feng, I.U. Idehenre, D.R. Evans, M.W. Kanan, Molecular catalysis at polarized interfaces created by ferroelectric $BaTiO_3$, Chem. Sci. 8 (2017) 2790–2794.
[16] L.C. Tănase, L.E. Abramiuc, C.M. Teodorescu, Photoelectron spectroscopic and microspectroscopic probes of ferroelectrics, AIP Conf. Proc. 1916 (1–10) (2017) 030001.
[17] S.V. Kalinin, D.A. Bonnell, T. Alvarez, X. Lei, Z. Hu, J.H. Ferris, Q. Zhang, S. Dunn, Atomic polarization and local reactivity on ferroelectric surfaces: a new route toward complex nanostructures, Nano Lett. 2 (2002) 589–593.
[18] L. Pintilie, M. Alexe, Metal-ferroelectric-metal heterostructures with Schottky contacts. I. Influence of the ferroelectric properties, J. Appl. Phys. 98 (1–8) (2005) 124103.
[19] A. Kakekhani, S. Ismail-Beigi, E.I. Altman, Ferroelectrics: A pathway to switchable surface chemistry and catalysis, Surf. Sci. 650 (2016) 302–316.
[20] T.T. Zhang, W.Y. Lei, P. Liu, J.A. Rodriguez, J.G. Yu, Y. Qi, G. Liu, M.H. Liu, Insights into the structure–photoreactivity relationships in well-defined perovskite ferroelectric $KNbO_3$ nanowires, Chem. Sci. 6 (2015) 4118–4123.
[21] D. Li, M.H. Zhao, J. Garra, A.M. Kolpak, A.M. Rappe, D.A. Bonnell, J.M. Vohs, Direct *in situ* determination of the polarization dependence of physisorption on ferroelectric surfaces, Nature Mater. 7 (2008) 473–477.
[22] S. Nassreddine, F. Morfin, G. Niu, B. Vilquin, F. Gaillard, L. Piccolo, Application of a sensitive catalytic reactor to the study of CO oxidation over $SrTiO_3$(100) and $BaTiO_3/SrTiO_3$(100) ferroelectric surfaces, Surf. Interface Anal. 46 (2014) 721–725.
[23] E. Ramos-Moore, D. Lederman, A.L. Cabrera, Modification of ferroelectric hysteresis in $Pb(Nb,Zr,Ti)O_3$ thin films induced by CO_2 adsorption, Appl. Surf. Sci. 258 (2011) 1181–1183.
[24] Q. Fu, X.J. Wang, C.Y. Li, Y. Sui, Y.P. Han, Z. Lv, B. Song, P. Xu, Enhanced photocatalytic activity on polarized ferroelectric $KNbO_3$, RSC Adv. 6 (2016) 108883–108887.
[25] S. Dunn, P.M. Jones, D.E. Gallardo, Photochemical growth of silver nanoparticles on c- and c+ domains on lead zirconate titanate thin films, J. Am. Chem. Soc. 129 (2007) 8724–8728.
[26] N. Domingo, E. Pach, K. Cordero-Edwards, V. Pérez-Dieste, C. Escudero, A. Verdaguer, Water adsorption, dissociation and oxidation on $SrTiO_3$ and ferroelectric surfaces revealed by ambient pressure X-ray photoelectron spectroscopy, Phys. Chem. Chem. Phys. 21 (2019) 4920–4930.
[27] S.C. Tu, Y.H. Zhang, A.H. Reshak, S. Auluck, L.Q. Ye, X.P. Han, T.Y. Ma, H.W. Huang, Ferroelectric polarization promoted bulk charge separation for highly efficient CO_2 photoreduction of $SrBi_4Ti_4O_{15}$, Nano Energy 56 (2019) 840–850.
[28] E. Ramos-Moore, P. Ferrari, D.E. Diaz-Droguett, D. Lederman, J.T. Evans, Raman and x-ray photoelectron spectroscopy study of ferroelectric switching in $Pb(Nb,Zr,Ti)O_3$ thin films, J. Appl. Phys. 111 (1–8) (2012) 014108.
[29] N.G. Apostol, G.A. Lungu, I.C. Bucur, C.A. Tache, L. Hrib, L. Pintilie, D. Macovei, C.M. Teodorescu, Non-interacting, sp^2 hybridized carbon layers on ferroelectric lead zirco-titanate, RSC Adv. 6 (2016) 67883–67887.
[30] T. Engel, G. Ertl, Elementary steps in the catalytic oxidation of carbon monoxide on platinum metals, Adv. Catal. 28 (1979) 1–78.
[31] T.T. Zhang, W.Y. Lei, P. Liu, J.A. Rodriguez, J.G. Yu, Y. Qi, G. Liu, M.H. Liu, Organic pollutant photodecomposition by $Ag/KNbO_3$ nanocomposites: a combined experimental and theoretical study, J. Phys. Chem. C 120 (2016) 2777–2786.
[32] J.Y. Lan, X.M. Zhou, G. Liu, J.C. Zhang, L.J. Zhi, G.J. Nie, Enhancing photocatalytic activity of one-dimensional KNbO3 nanowires by Au nanoparticles under ultraviolet and visible-light, Nanoscale 3 (2011) 5161–5167.
[33] N.G. Apostol, L.E. Stoflea, G.A. Lungu, C. Chirila, L. Trupina, R.F. Negrea, C. Ghica, L. Pintilie, C.M. Teodorescu, Charge transfer and band bending at $Au/Pb(Zr,Ti)O_3$ interfaces investigated by photoelectron spectroscopy, Appl. Surf. Sci. 273 (2013) 415–425.
[34] D.G. Popescu, M.A. Huşanu, L. Trupină, L. Hrib, L. Pintilie, A. Barinov, S. Lizzit, P. Lacovig, C.M. Teodorescu, Spectro-microscopic photoemission evidence of charge uncompensated areas in $Pb(Zr,Ti)O_3$(001) layers, Phys. Chem. Chem. Phys.

17 (2015) 509–520.
[35] L.E. Abramiuc, L.C. Tănase, A. Barinov, N.G. Apostol, C. Chirilă, L. Trupină, L. Pintilie, C.M. Teodorescu, Polarization landscape effects in soft X-ray-induced surface chemical decomposition of lead zirco-titanate, evidenced by photoelectron spectromicroscopy, Nanoscale 9 (2017) 11055–11067.
[36] E. Ramos-Moore, D.E. Diaz-Droguett, P. Spring, J.T. Evans, A.L. Cabrera, Generation of oxygen vacancies in the surface of ferroelectric $Pb(Nb,Zr,Ti)O_3$, Appl. Surf. Sci. 257 (2011) 4695–4698.
[37] L. Mokoena, G. Pattrick, M.S. Scurell, Catalytic activity of gold-perovskite catalysts in the oxidation of carbon monoxide, Gold Bull. 49 (2016) 35–44.
[38] F. Chen, A. Klein, Polarization dependence of Schottky barrier heights at interfaces of ferroelectrics determined by photoelectron spectroscopy, Phys. Rev. B 86 (1–7) (2012) 094105.
[39] L. Pintilie, C. Ghica, C.M. Teodorescu, I. Pintilie, C. Chirila, I. Pasuk, L. Trupina, L. Hrib, A.G. Boni, N.G. Apostol, L.E. Abramiuc, R. Negrea, M. Stefan, D. Ghica, Polarization induced self-doping in epitaxial $Pb(Zr_{0.20}Ti_{0.80})O_3$ thin films, Sci. Rep. 5 (1–14) (2015) 14974.
[40] C.M. Teodorescu, J.M. Esteva, R.C. Karnatak, A. El Afif, An approximation of the Voigt I profile for the fitting of experimental x-ray absorption data, Nucl. Instrum. Methods Phys. Res. A 345 (1994) 141–147.
[41] D. Mardare, D. Luca, C.M. Teodorescu, D. Macovei, On the hydrophilicity of nitrogen-doped TiO_2 thin films, Surf. Sci. 601 (2007) 4515–4520.
[42] D. Luca, C.M. Teodorescu, R. Apetrei, D. Macovei, D. Mardare, Preparation and characterization of increased-efficiency photocatalytic TiO2–$2_x$$N_x$ thin films, Thin Solid Films 515 (2007) 8605–8610.
[43] J.J. Yeh, I. Lindau, Atomic subshell photoionization cross sections and asymmetry parameters: $1 \leq Z \leq 103$, Atomic Data Nucl. Data Tables 32 (1985) 1–155 See also https://vuo.elettra.eu/services/elements/WebElements.html.
[44] L.C. Tănase, L.E. Abramiuc, D.G. Popescu, A.-M. Trandafir, N.G. Apostol, I.C. Bucur, L. Hrib, L. Pintilie, I. Pasuk, L. Trupină, C.M. Teodorescu, Polarization orientation in lead zirco-titanate (001) thin films driven by the interface with the substrate, Phys. Rev. Applied 10 (1–19) (2018) 034020.
[45] M. Iliut, C. Leordean, V. Canpean, C.M. Teodorescu, S. Astilean, A new green, ascorbic acid-assisted method for versatile synthesis of Au-graphene hybrids as efficient surface-enhanced Raman scattering platforms, J. Mater. Chem. C Mater. Opt. Electron. Devices 1 (2013) 4094–4104.
[46] A. Pancotti, J. Wang, P. Chen, L. Tortech, C.M. Teodorescu, E. Frantzeskakis, N. Barrett, X-ray photoelectron diffraction study of relaxation and rumpling of ferroelectric domains in $BaTiO_3$(001), Phys. Rev. B 87 (1–10) (2013) 184116.
[47] N.G. Apostol, L.E. Ştoflea, L.C. Tănase, I.C. Bucur, C. Chirilă, R.F. Negrea, C.M. Teodorescu, Band bending at copper and gold interfaces with ferroelectric Pb(Zr,Ti)O_3 investigated by photoelectron spectroscopy, Appl. Surf. Sci. 354 (2015) 459–468.
[48] N.H. Turner, A.M. Single, Determination of peak positions and areas from wide-scan XPS spectra, Surf. Interface Anal. 15 (1990) 215–222.
[49] J.J. Pireaux, M. Leihr, P.A. Thiry, J.P. Delrue, R. Caudano, Electron spectroscopic characterization of oxygen adsorption on gold surfaces. II. Production of gold oxide in oxygen DC reactive sputtering, Surf. Sci. 141 (1984) 221–232.
[50] V.I. Bukhtiyarov, V.V. Kaichev, I.P. Prosvirin, X-ray photoelectron spectroscopy as a tool for *in-situ* study of the mechanisms of heterogeneous catalytic reactions, Top. Catal. 32 (2005) 3–15.
[51] MTDATA – Phase Diagram Software from the National Physical Laboratory, (2019) accessed August 22 http://resource.npl.co.uk/mtdata/phdiagrams/aupb.htm.
[52] M.O. Krause, J.H. Oliver, Natural widths of atomic K and L levels, Kα X-ray lines and several KLL Auger lines, J. Phys. Chem. Ref. Data 8 (1979) 329–338.
[53] M. Neeb, J.-E. Rubensson, M. Biermann, W. Eberhardt, Coherent excitation of vibrational wave functions observed in core hole decay spectra of O_2, N_2 and CO, J. El. Spectrosc. Relat. Phenom. 67 (1994) 261–274.
[54] C.M. Teodorescu, Image molecular dipoles in surface enhanced raman scattering, Phys. Chem. Chem. Phys. 17 (2015) 21302–21314.
[55] D.R. Lide, et al. (Ed.), Handbook of Chemistry and Physics, 75th edition, CRC Press, Boca Raton, 1995.
[56] H.G. Howell, Dissociation energy of carbon monoxide, Nature 163 (1949) 773.